

Tribol Lett (2014) 56:457–470  
DOI 10.1007/s11249-014-0422-0

ORIGINAL PAPER

# Relationship Between the Friction and Microscopic Contact Behavior of a Medical Compression Stocking at Different Strains

W. Ke · G.-M. Rotaru · J. Y. Hu · X. Ding ·  
R. M. Rossi · S. Derler

Received: 20 July 2014 / Accepted: 22 September 2014 / Published online: 8 October 2014  
© Springer Science+Business Media New York 2014

**Abstract** The contact and friction behavior of a medical compression stocking (MCS) under different strains was investigated in friction and compression experiments against a mechanical skin model. In addition, the 3D topography of the MCS surfaces was analyzed in order to study the relationship between macroscopic friction and microscopic surface properties. The load dependence of friction coefficients was found to be in accordance with the adhesion friction model. The surface structure of MCS samples was considerably changed when varying the strain state, while friction coefficients remained comparable, indicating real contact areas independent of strain on the microscopic level. The experimental findings could be confirmed and explained on the basis of the microscopic surface analyses, when interpreting the fabric surfaces to be composed of numerous individual round asperities obeying the Hertz contact model.

**Keywords** Skin tribology · Medical compression stocking · Surface topography · Microscopic contact area · Macroscopic friction

## 1 Introduction

Medical compression stockings (MCSs) are elastic textiles which are widely used for the prophylaxis and therapeutic treatment of venous disorders in the human lower extremities [1–3]. In addition, compression stockings are used as training aids for athletes of various sport disciplines [4]. By providing an external and controlled pressure gradient along the leg, stockings can help to reduce the effects of venous insufficiency and improve the lower limb venous blood return [5–8].

In order to be effective, MCSs have to meet requirements regarding their physical properties as well as comfort and acceptability. User surveys show that a common problem with MCSs in practice is the putting on process [9]. In particular, it is difficult to pull the narrow ankle region of a compression stocking over the wider heel area of the foot. In the stretched condition, the stocking imposes a high contact pressure on the foot skin, leading to high friction forces that counteract the forces applied to pull on the stocking. Thus, the friction behavior of MCSs in contact with the skin is an important factor, and it is expected that a low friction coefficient (COF) improves the ease of handling. On the other hand, the friction of a MCS has to be sufficiently high in order to prevent slipping and displacements when placed in the correct wearing position.

A MCS sliding on human skin represents a complex tribological system that so far has not been systematically investigated in detail. Previous studies focused on the compressive properties and therapeutic effects of MCSs [10–13], ignoring the friction properties. Therefore, the friction behavior of MCSs on skin is still unclear, and it is unknown how the friction coefficient varies in different situations (putting on, wearing) and as a function of the strain state of the textile.

W. Ke · G.-M. Rotaru · R. M. Rossi · S. Derler (✉)  
Laboratory for Protection and Physiology, Empa, Swiss Federal  
Laboratories for Materials Science and Technology,  
Lerchenfeldstrasse 5, 9014 St. Gallen, Switzerland  
e-mail: siegfried.derler@empa.ch

W. Ke · J. Y. Hu · X. Ding  
College of Textiles, Donghua University, Shanghai 201620,  
People's Republic of China

Studies on the friction of human skin [14, 15] provided information on the influencing factors, indicating that skin hydration and the surface properties of the contacting materials are major parameters. Elevated skin hydration is commonly believed to increase skin friction by smoothing and softening skin roughness asperities, leading to a greater real contact area to a counter-surface. Concerning the influence of the surface roughness of a contacting material on skin friction, there is no consistent view in the literature. Skedung et al. [16] and Hendriks and Franklin [15] found that the friction coefficient of dry skin decreases with increasing material surface roughness, while Tomlinson et al. [17] reported that the friction coefficient between skin and rather rough surfaces increases with roughness. Masen [18] proposed a bell-shaped relationship between the roughness of a counter-surface and the friction coefficient of hydrated skin. The different experimental findings indicate that the influence of surface topography on skin friction is intricate and depends on the friction mechanisms arising on the microscopic level, which in turn are ultimately determined by the interfacial contact parameters and resulting real contact area.

MCSs are characterized by a specific surface structure which is given by the textile construction. As the surface topography varies with the applied tensile stress, it is a question whether topographical changes induced by varying strain have an influence on the friction between a MCS and skin. We hypothesized that changes in the MCS surface topography alter the real contact area against a counter-surface and, as a consequence, also the associated friction coefficient.

The objective of the present study was to investigate the friction behavior of a typical MCS in contact with a skin model by studying the influence of changes in the MCS surface topography on friction. In order to gradually change the surface structure of the MCS, a series of strains were applied on the samples simulating different wearing conditions. Macroscopic friction coefficients between the samples and the skin model were measured using a linear reciprocating tribometer, while the elastic properties were obtained in compression tests. The contact behavior of MCS samples at the microscopic level was analyzed on the basis of 3D surface topography data measured by means of a digital microscope. For comparison, two theoretical models were adopted to predict the real contact area of the MCS surfaces against a smooth substrate from basic geometrical and mechanical parameters related to the textile construction and composing fibers.

## 2 Materials and Methods

### 2.1 MCS Samples

A typical, commercially available knitted MCS of compression class I (low compression intensity) was investigated

**Table 1** Specification of the MCS and constituent yarns

|             | Structure         | Fiber materials           |
|-------------|-------------------|---------------------------|
| Loop yarn   | Core yarn         | Lycra (mono), 44 dtex     |
|             | 1st covering yarn | Polyamide, 10 dtex (33 f) |
|             | 2nd covering yarn | Polyamide, 10 dtex (33 f) |
| Inlaid yarn | Core yarn         | Lycra (mono), 475 dtex    |
|             | 1st covering yarn | Polyamide, 7 dtex (22 f)  |
|             | 2nd covering yarn | Cotton, 435 dtex          |

The fineness of yarns and textile fibers is given in dtex, corresponding to the mass in grams per 10 km. It is an indirect measure for the fiber diameter. If a yarn is composed of filaments (f), their number is given in brackets

in this study. According to the widely accepted standard RAL-GZ 387/1 [19], compression hosiery of class I exerts a pressure of 2.4–2.8 kPa on the leg in the ankle area. The structure of the MCS differs from traditional socks and includes two components: the inlaid yarns and the knitted loop yarns. The inlaid yarn is usually a synthetic elastic yarn with or without covering filaments which is inserted between the knitted loop yarns. The inlaid yarns play a key role in forming the surface topography of the inner side of the MCS in contact with the skin of the leg (Fig. 3), because they are around ten times thicker than the loop yarns (Table 1). Both inlaid and loop yarns include three layers (core yarn, 1st covering yarn and 2nd covering yarn). Details of the yarns are listed in Table 1.

Due to the negative fit of MCSs, stresses and deformations occur along more than one axial direction in practical use, and the range of elongation usually lies between 15 and 120 % [19]. The geometrical shape of the human foot implies that the ankle area of a MCS is typically stretched between 30 and 40 % when pulled over the heel area. Therefore, the extension tests of the samples were arranged as 0, 25, 50, and 75 % in both inlaid yarn direction (*i*-direction) and perpendicular direction (*p*-direction), corresponding to the circumferential and length direction of the MCS, respectively.

To obtain different strains, the samples were stretched from the original length to a given loaded length. The setup for MCS preparation is shown in Fig. 1. The stretched samples were fixed to metal plates for microscopic analyses (Sect. 2.3) or to the sample holder for friction testing (Sect. 2.2) using double-adhesive tape and ensuring an even strain distribution parallel and perpendicular to the direction of the tensile force. The extensibility of the samples is

$$\varepsilon = \frac{L_1 - L_0}{L_0} \times 100 \% \quad (1)$$

where  $L_0$  is the original and  $L_1$  the extended length, which was set at 37 mm for convenience in sample preparation.

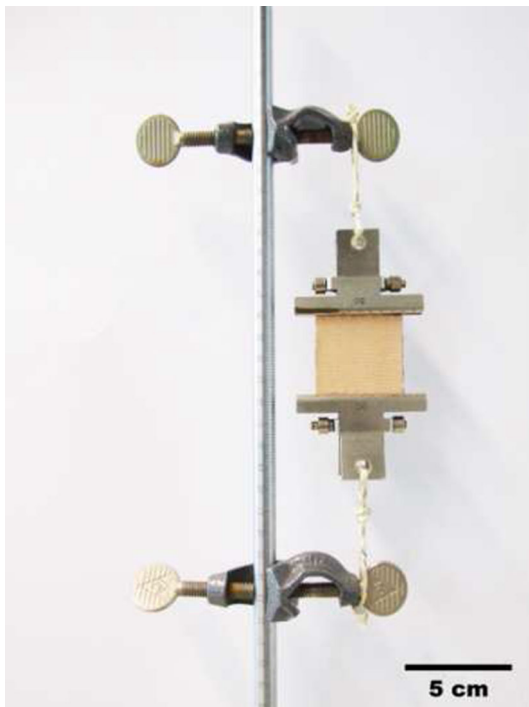


**Fig. 1** Setup for MCS sample preparation

## 2.2 Friction Measurements

A previously developed textile friction analyser (TFA) [20] was used to investigate the friction behavior of the MCS samples under contact conditions simulating those in the limb skin/MCS interface. Figure 2 illustrates the TFA measurements. The slider is flat and circular with a diameter of 28.5 mm, leading to a surface area of around 6.4 cm<sup>2</sup>. MCS samples attached to the slider were rubbed with the reciprocating support covered with a polyurethane (PUR) sheet material (thickness  $1.005 \pm 0.013$  mm) which was taken as a mechanical skin model. This specific PUR material was chosen from a range of materials investigated previously [21] because its surface ( $R_a = 0.21 \pm 0.02$  μm) is smooth compared to the MCS and its hardness (shore A  $70.2 \pm 0.4$ ) seems suitable to simulate the skin in the heel area that appears relatively hard due to the underlying calcaneus bone.

During the friction measurements, the MCS samples remained stationary while the mechanical skin model on its metallic support base underwent 550 linear friction cycles with a stroke of 20 mm and a frequency of 1.25 Hz. The normal and friction forces were measured continuously and simultaneously; a typical force–time signal for one friction cycle is shown in Fig. 2b. Friction coefficients were determined for all friction cycles, and mean values and standard deviations were calculated over sequences of 50 cycles.

To explore the load dependence of MCS friction, normal loads of 0.5, 1, 2, 4 and 8 N were applied. These normal forces corresponded to contact pressures between 0.8 and 12.5 kPa, including the pressures exerted by an MCS of compression class I during wearing (2.4–2.8 kPa) [19] as well as elevated pressures expected during pulling on. The sliding direction was parallel to the  $p$ -direction, along the length axis of the leg. The friction measurements were carried out under dry and wet conditions in a laboratory with standard climate ( $20 \pm 1$  °C and  $65 \pm 2$  % relative humidity). All samples were preconditioned for 24 h in the laboratory climate before testing. Wet conditions were produced by immersing the MCS sample in deionized water for 1 min and removing the excess water using a dry tissue before a measurement. For each experimental configuration (combination of strain state, normal force and dry or wet condition), one fabric sample was investigated.

## 2.3 Surface Characterization

A digital optical microscope (Keyence, VHX-1000, Osaka, Japan) was used for the surface analysis of MCS samples at various strains. The inner surface of MCS which is next to the skin was taken for optical microscopic images and 3D topography analyses, using a magnification of 100. The 3D surface topography images were scanned by using a vertical increment of 10 μm. For each sample, several images from different parts were analyzed. Figure 3 shows optical images and 3D surface topographies of MCS samples in the unstretched state and stretched in two directions. It can be seen that the texture and surface topography of MCS samples significantly changed under varying strains.

To determine the surface variations in detail, geometrical parameters such as the difference in height between peaks and valleys, the distance between two inlaid yarns (spatial period) and the radii of curvature of the inlaid yarns were analyzed. The surface topographical data for the MCS samples at different strains were used to analyse the contact behavior against a smooth counter-surface. In particular, the microscopic contact area was estimated as a function of displacement normal to the interface by analyzing the height dependence of the material ratio within the textile (Abbott–Firestone curve). This method was recently described in connection with fabrics for medical bed sheets [22].

## 2.4 Compression Tests

Compression measurements were carried out to determine the contact behavior and elastic properties of MCS samples under various strains using a universal materials testing machine (Zwick 100, Zurich, Switzerland). The contact conditions were consistent with the previous friction tests

**Fig. 2** Friction measurements. **a** Schematic illustration of the TFA. **b** Typical force–time curve of one friction cycle. Friction coefficients are determined for all individual sliding movements

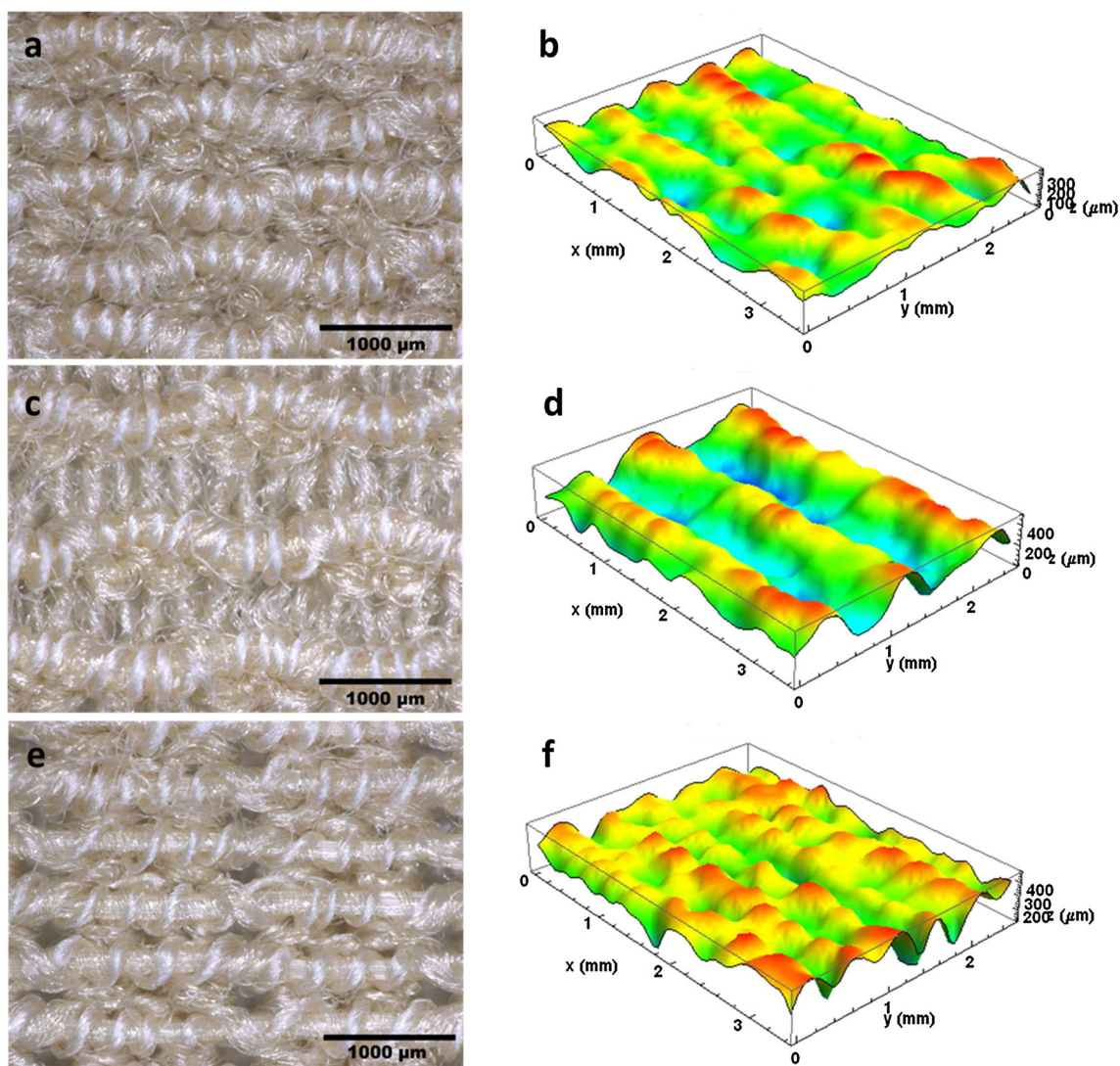
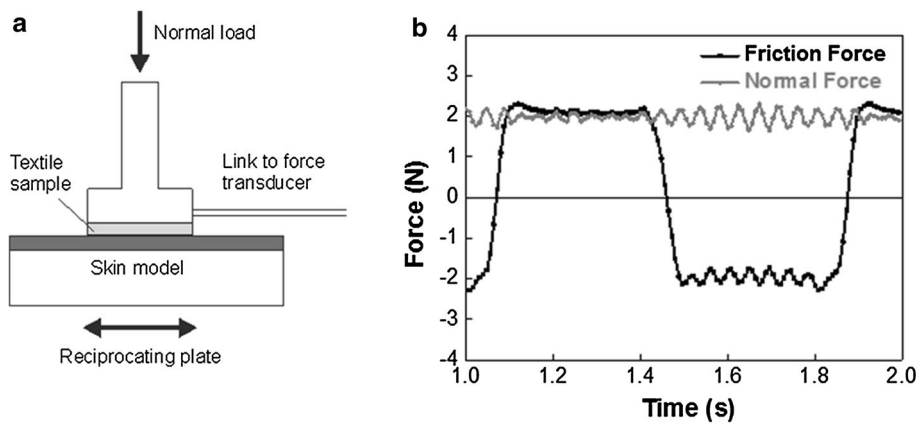


**Fig. 3** Optical microscopic images (**a**, **c**, **e**) and corresponding surface topography images (**b**, **d**, **f**) of MCS samples at strains of 0 and 75%. The *x*- and *y*-axes in the topographical plots correspond to

the horizontal and vertical direction in the optical images, respectively. **a** and **b** Unstretched state (0%); **c** and **d** 75% stretched in *p*-direction; **e** and **f** 75% stretched in *i*-direction

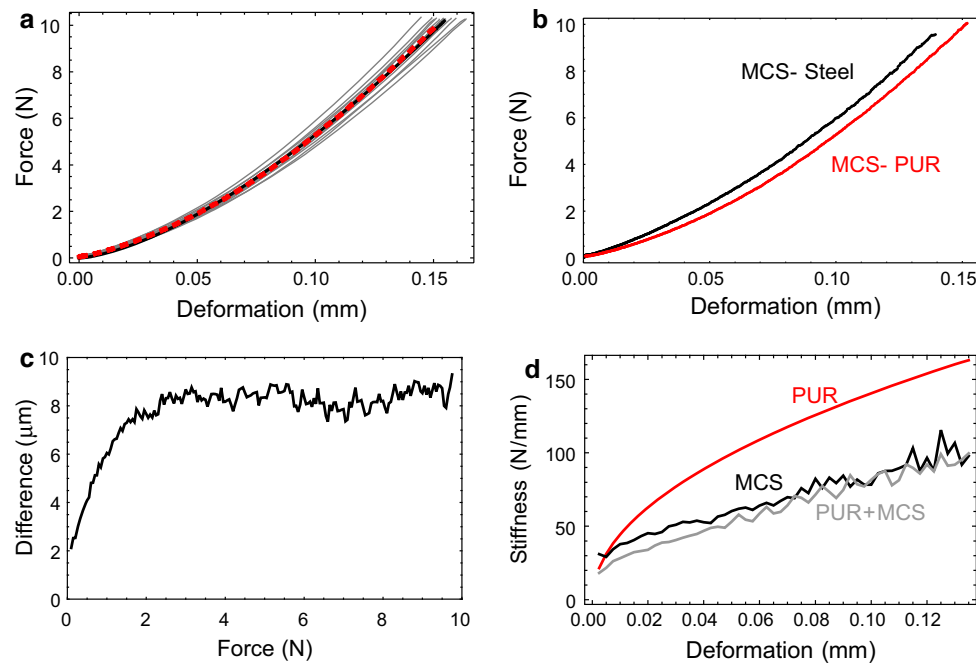


**Fig. 4** Results and analysis of compression tests with unstretched MCS samples. **a** Force–deformation curves measured for four samples compressed against the PUR skin model. The *thin lines* represent the results of 12 individual loading cycles, the *thick dashed line* is the average curve. The *thick solid line* shows a data fit assuming that the force is proportional to the deformation to the

(Sect. 2.2), using the same sample holder and fixation by means of adhesive tape. Compression tests with MCS samples were carried out against a rigid steel plate alone and covered with a skin model, a PUR sheet material with a thickness of  $1.005 \pm 0.013$  mm.

For each strain state, three to four MCS samples were investigated. Each measurement included four cyclic compression tests, in which the normal force was increased from a preload of 0.1 N to around 10 N with a compression rate of 5 mm/min. The force–deformation curve of the first compression cycle systematically deviated from those of the three subsequent cycles showing repeatable results. A possible reason is that slight fiber reorientations took place during the first loading cycle, leading to small residual deformations of the MCS samples. Therefore, the force–deformation curves from the last three loading cycles were analyzed.

Figure 4 shows force–deformation curves measured in compression tests for the example of the unstretched MCS fabric. The detailed data analysis is based on average force–deformation curves (a). The comparison of results obtained in compression tests against rigid steel and the PUR sheet (b) indicates the order of magnitude of the indentation of textile surface asperities into the PUR material during compression tests (c). Information on the

power of  $3/2$ . **b** Average curves obtained in compression tests against steel and PUR. **c** Difference of the deformation of the samples on PUR and steel as a function of compression force. **d** Stiffness as a function of deformation for the unstretched MCS fabric, the PUR sheet material and the combination MCS + PUR by determining local slopes to curves as shown in **b**

**Table 2** Thickness of uncompressed MCS samples for different strains, measured by means of a micrometer device

| Sample                      | Thickness (mm)    |
|-----------------------------|-------------------|
| Unstretched                 | $0.775 \pm 0.013$ |
| 25 % in <i>p</i> -direction | $0.680 \pm 0.016$ |
| 50 % in <i>p</i> -direction | $0.630 \pm 0.029$ |
| 75 % in <i>p</i> -direction | $0.563 \pm 0.022$ |
| 25 % in <i>i</i> -direction | $0.675 \pm 0.024$ |
| 50 % in <i>i</i> -direction | $0.625 \pm 0.021$ |
| 75 % in <i>i</i> -direction | $0.565 \pm 0.019$ |

Mean values and standard deviations of 4 measurements

stiffness of MCS fabrics alone and in combination with the PUR film is obtained by determining local slopes to average force–deformation curves (d). Because the stiffness ( $k$ ) and the elastic modulus ( $E$ ) are related by  $E = \frac{T_0}{A_0} k$  (where  $T_0$  is the initial thickness and  $A_0$  the sample area), it is possible to estimate the elastic modulus directly from the values for the stiffness. While the sample area  $A_0$  was constant for all investigated MCS samples ( $6.38 \text{ cm}^2$ ), the initial thickness of the samples linearly decreased with their strain state (Table 2). The results were comparable for samples stretched in *p*- and *i*-direction.

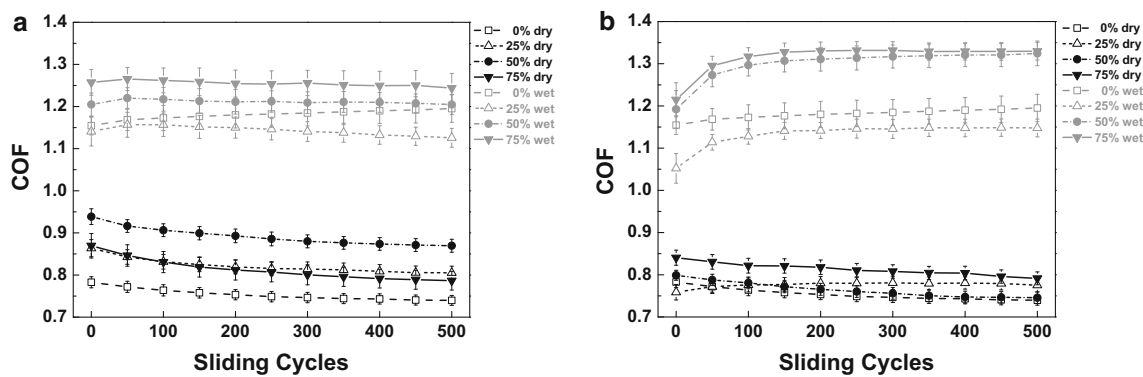


**Fig. 5** Dynamic friction coefficients as a function of sliding friction cycles for MCS samples at different strains **a** in *p*-direction and **b** in *i*-direction under dry and wet conditions (experiments with a normal load of 4 N)

### 3 Results

#### 3.1 Friction Between MCS and PUR

##### 3.1.1 Range and Variation of Friction Coefficients

Figure 5 shows the time dependence of friction coefficients of MCS samples measured under dry and wet conditions for the example of experiments at a normal load of 4 N. In many cases, slight running-in effects were observed during the initial phase of the friction experiments (up to about 100 friction cycles), while the subsequent friction coefficients remained practically constant, indicating stationary sliding friction. Therefore, in order to calculate global mean values and standard deviations of friction coefficients, the last 350 sliding cycles were taken into account.

Table 3 summarizes the measured sliding friction coefficients of MCSs for different strains and normal forces under dry and wet conditions. The mean friction coefficients ranged from 0.69 to 2.82 in the dry condition and from 0.95 to 5.21 in the wet condition. The results for samples stretched in *p*-direction and *i*-direction were comparable.

##### 3.1.2 Strain and Load Dependence of Friction Coefficients

The data in Table 3 indicate neither a systematic influence of the strain nor significant differences between the results for strains in *i*- and *p*-direction. On the other hand, the friction coefficients of all samples in both dry and wet conditions systematically decreased with increasing normal load. In the wet condition, there was a distinct decrease for normal forces from 0.5 to 2 N, followed by relatively constant friction coefficients at higher forces (with COF values somewhat above 1 at a normal force of 8 N). Under dry conditions, the initial decline was less pronounced and the friction coefficients stabilized at lower values (with

COF values below 1 at a normal force of 8 N). The highest COF values in the order of magnitude of 5 were observed for wet MCS samples at the smallest normal force. The observed systematic decrease of friction coefficients with increasing normal load is in accordance with the adhesion friction model. This will be further discussed in detail in Sect. 4.1.

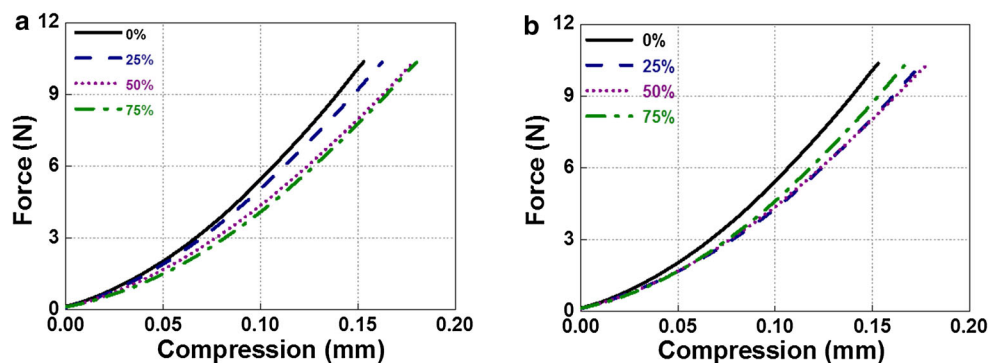
#### 3.2 Compression Behavior of MCS Fabrics

Average force–deformation curves of MCS samples compressed against the PUR skin model are shown in Fig. 6. The compression behavior of MCS fabrics was generally characterized by nonlinear force–deformation curves, indicating progressive stiffness with increasing compression. From the phenomenological point of view, all force–deformation curves were in good agreement with a power law with an exponent of 3/2, i.e.,  $F(d) \sim d^{3/2}$ . The steepest force–deformation curve was observed for the unstretched samples. The force–deformation curves gradually flattened for increasing strains in *p*-direction (Fig. 6a), but this systematic behavior was not seen for strains in *i*-direction (Fig. 6b).

Under the maximum normal load of 8 N as used in the friction measurements, the combined deformation of PUR and the unstretched MCS sample was 0.131 mm. For strains in *p*- and *i*-direction, the corresponding deformations ranged from 0.139 to 0.154 mm and from 0.145 to 0.152 mm, respectively. When compressed against a steel plate, the MCS samples systematically showed slightly smaller deformations. The average differences in compression tests of MCS samples against PUR and steel are shown as a function of the normal load in Fig. 7. In compression tests against PUR, the average deformation was up to 0.012 mm higher than that against steel. Because the PUR skin model is softer than steel, it is assumed that the indentation of textile surface asperities into the smooth

**Table 3** Mean  $\pm$  standard deviation of friction coefficients for MCS samples investigated at different strains and normal forces under dry and wet conditions

|                             | 0.5 N             | 1 N               | 2 N               | 4 N               | 8 N               |
|-----------------------------|-------------------|-------------------|-------------------|-------------------|-------------------|
| Dry condition               |                   |                   |                   |                   |                   |
| Unstretched                 | 1.835 $\pm$ 0.021 | 1.206 $\pm$ 0.008 | 0.840 $\pm$ 0.007 | 0.745 $\pm$ 0.005 | 0.745 $\pm$ 0.008 |
| 25 % in <i>p</i> -direction | 2.820 $\pm$ 0.050 | 1.226 $\pm$ 0.008 | 0.876 $\pm$ 0.004 | 0.812 $\pm$ 0.005 | 0.783 $\pm$ 0.004 |
| 50 % in <i>p</i> -direction | 1.646 $\pm$ 0.015 | 1.308 $\pm$ 0.018 | 1.039 $\pm$ 0.018 | 1.039 $\pm$ 0.018 | 0.898 $\pm$ 0.012 |
| 75 % in <i>p</i> -direction | 2.081 $\pm$ 0.033 | 1.218 $\pm$ 0.025 | 1.219 $\pm$ 0.022 | 1.083 $\pm$ 0.020 | 0.920 $\pm$ 0.015 |
| Unstretched                 | 1.896 $\pm$ 0.010 | 1.292 $\pm$ 0.007 | 1.009 $\pm$ 0.008 | 0.887 $\pm$ 0.005 | 0.801 $\pm$ 0.003 |
| 25 % in <i>i</i> -direction | 1.742 $\pm$ 0.025 | 1.017 $\pm$ 0.008 | 0.898 $\pm$ 0.004 | 0.779 $\pm$ 0.002 | 0.698 $\pm$ 0.004 |
| 50 % in <i>i</i> -direction | 1.804 $\pm$ 0.013 | 1.115 $\pm$ 0.007 | 0.776 $\pm$ 0.005 | 0.753 $\pm$ 0.008 | 0.723 $\pm$ 0.008 |
| 75 % in <i>i</i> -direction | 1.390 $\pm$ 0.011 | 1.098 $\pm$ 0.009 | 0.934 $\pm$ 0.010 | 0.805 $\pm$ 0.009 | 0.692 $\pm$ 0.005 |
| Wet condition               |                   |                   |                   |                   |                   |
| Unstretched                 | 3.912 $\pm$ 0.042 | 2.429 $\pm$ 0.017 | 1.635 $\pm$ 0.005 | 1.187 $\pm$ 0.005 | 1.072 $\pm$ 0.005 |
| 25 % in <i>p</i> -direction | 4.943 $\pm$ 0.112 | 2.451 $\pm$ 0.022 | 1.389 $\pm$ 0.010 | 1.138 $\pm$ 0.009 | 0.947 $\pm$ 0.006 |
| 50 % in <i>p</i> -direction | 2.193 $\pm$ 0.040 | 2.201 $\pm$ 0.021 | 1.417 $\pm$ 0.009 | 1.209 $\pm$ 0.002 | 1.115 $\pm$ 0.001 |
| 75 % in <i>p</i> -direction | 2.736 $\pm$ 0.016 | 1.911 $\pm$ 0.012 | 1.616 $\pm$ 0.007 | 1.251 $\pm$ 0.004 | 1.176 $\pm$ 0.004 |
| Unstretched                 | 4.701 $\pm$ 0.412 | 2.046 $\pm$ 0.014 | 1.397 $\pm$ 0.012 | 1.159 $\pm$ 0.002 | 1.086 $\pm$ 0.003 |
| 25 % in <i>i</i> -direction | 4.120 $\pm$ 0.006 | 2.126 $\pm$ 0.023 | 1.393 $\pm$ 0.004 | 1.147 $\pm$ 0.002 | 1.058 $\pm$ 0.004 |
| 50 % in <i>i</i> -direction | 2.865 $\pm$ 0.047 | 2.610 $\pm$ 0.015 | 1.799 $\pm$ 0.003 | 1.318 $\pm$ 0.005 | 1.038 $\pm$ 0.003 |
| 75 % in <i>i</i> -direction | 5.210 $\pm$ 0.053 | 2.025 $\pm$ 0.020 | 1.813 $\pm$ 0.006 | 1.330 $\pm$ 0.001 | 1.069 $\pm$ 0.013 |

**Fig. 6** Average force–deformation curves of MCS samples at different strains **a** in *p*-direction and **b** in *i*-direction when compressed against the PUR skin model

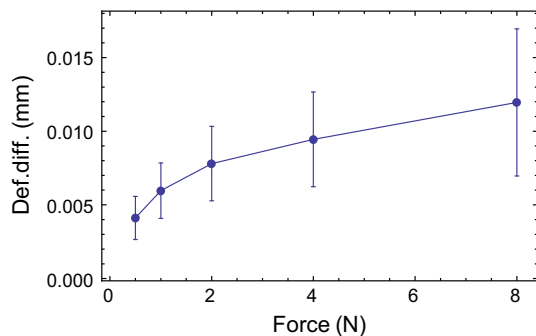
PUR surface plays a role in the compression of MCS against PUR and that the results in Fig. 7 indicate the order of magnitude of the indentation or penetration depth.

Figure 8 shows the results for the compressive elastic modulus of MCS samples for different strains and normal loads. Because of the nonlinear force–deformation relations shown in Fig. 6, the elastic modulus increases with normal load. It can also be noticed that for a given load, the elastic modulus linearly decreases with the strain of the MCS fabric. In other words, the textiles appear softer when stretched, which could result from a decreased material density.

### 3.3 Microscopic Analyses of MCS Surfaces

#### 3.3.1 Geometrical Parameters of MCS Samples at Different Strains

Microscopic and topographical images (Fig. 3) show that the texture of MCS surfaces changes significantly under the influence of strains. To characterize the variation of the MCS surface structure with increasing strain in detail, various geometrical parameters were determined from microscopic surface topography images by analyzing cross-sectional profiles (Fig. 9).



**Fig. 7** Average differences in the deformation of MCS samples when compressed against PUR and steel as a function of the normal load

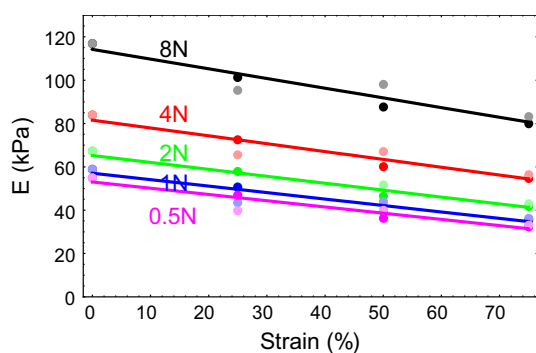


**Fig. 8** Elastic moduli of MCS samples determined from compression tests against PUR for different strains and normal forces. Results for strains in *p*-direction are shown as *dark symbols*, results for strains in *i*-direction as *bright symbols*

The surface of the unstretched samples appears relatively flat. The protruding inlaid yarns are arranged close to each other (see also Fig. 3). If stretched in *p*-direction, the inlaid yarns are separated so that their average distance linearly increases with strain (Fig. 10a). At the same time, the inlaid yarns gradually emerge, so that the peak-to-valley height increases by 50 % from 268 to 398  $\mu\text{m}$  (Fig. 10b). In contrast, when stretching in *i*-direction, the inlaid yarns are extended and oriented to the strain direction, while the MCS becomes flatter and the peak-to-valley height decreases by 40 % from 268  $\mu\text{m}$  down to 167  $\mu\text{m}$  (Fig. 10b). For strains in *i*-direction, the inlaid yarn distance remains approximately constant (Fig. 10a). The average radius of curvature of the inlaid yarns is 180  $\mu\text{m}$  and does not depend on the applied strain.

### 3.3.2 Material Ratio of MCS Surfaces as a Function of Height

The analysis of the microscopic 3D surface topography of MCS samples provides detailed information on the

material distribution within the uncompressed MCSs. Of particular interest is the material distribution at the highest regions of the MCS surfaces which are decisive for the contact behavior on the microscopic level (together with the compression properties of the textile described in Sect. 3.2).

Therefore, the topographical data of MCS surfaces were analyzed in the regions of the local maxima. It was assumed that due to the flexibility of the textile material, the local maxima with heights above the average are simultaneously coming into contact with the smooth PUR counter-surface, thereby producing a microscopic contact area to the counter-surface which increases with the compression of the MCS and is primarily given by the material distribution within the highest surface elevations of the textile. Figure 11 shows the material ratio, i.e., the fraction of material above a cross section at a certain height of the surface, as a function of the vertical axis for MCS fabrics at different strains. For limited surface deformations, the material ratio can be associated with the contact area that is formed with a smooth counter-surface during mechanical contact. Fabric surfaces were considered as composed of roundish asperities that during mechanical contact with a smooth surface either penetrate into the counter-material (if the textile is harder) or are compressed against the counter-material (if the textile is softer) [22]. It was found that for small vertical deformations, both cases (either penetration or compression) predict a similar dependence of the contact area as a function of the deformation and that the material ratio of the textile represents a realistic estimate for the contact area.

The results in Fig. 11 indicate the highest material ratios for the surfaces of unstretched MCS samples. For the surfaces of strained fabrics, a trend toward lower material ratios can be observed, which is more pronounced in *p*-direction. This trend is correlated with the surface changes described in Sect. 3.3.1. The material ratios generally show a linear increase with the height coordinate up to values of 60  $\mu\text{m}$ . For smaller deformations (up to 20  $\mu\text{m}$ ), the material ratios were comparable for all MCS surfaces.

## 4 Discussion

### 4.1 Friction Mechanisms

The friction coefficients of all MCS samples ranged from 0.69 to 5.2 and strongly depended on the presence of interfacial water and the applied normal load. The friction coefficients generally decreased with increasing load, and the trends were more pronounced for wet conditions. In the wet condition, the COFs were a factor of 1.5–2 higher than

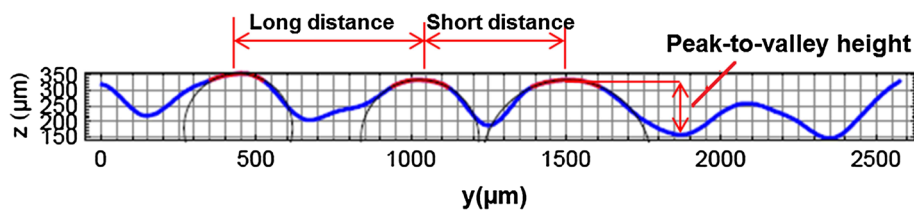


**Fig. 9** Cross-sectional profile (*blue curve*) extracted from the topographical data of an unstretched MCS sample in order to determine the peak-to-valley height differences, inlaid yarn distances and radii of curvature of the inlaid yarns. The inlaid yarn distance was

calculated as the average of long and short distances between two periodic inlaid yarns, and the radii of curvature were determined by fitting circles to the peak regions (highest 20 μm) of the inlaid yarns (*red curve segments*) (Color figure online)

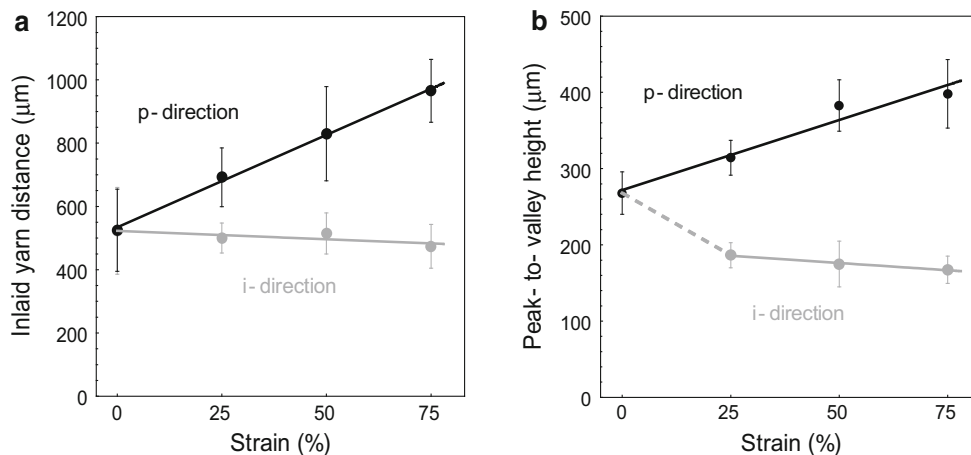


**Fig. 10** Geometrical parameters of MCS samples at different strains: **a** inlaid yarn distance and **b** peak-to-valley height

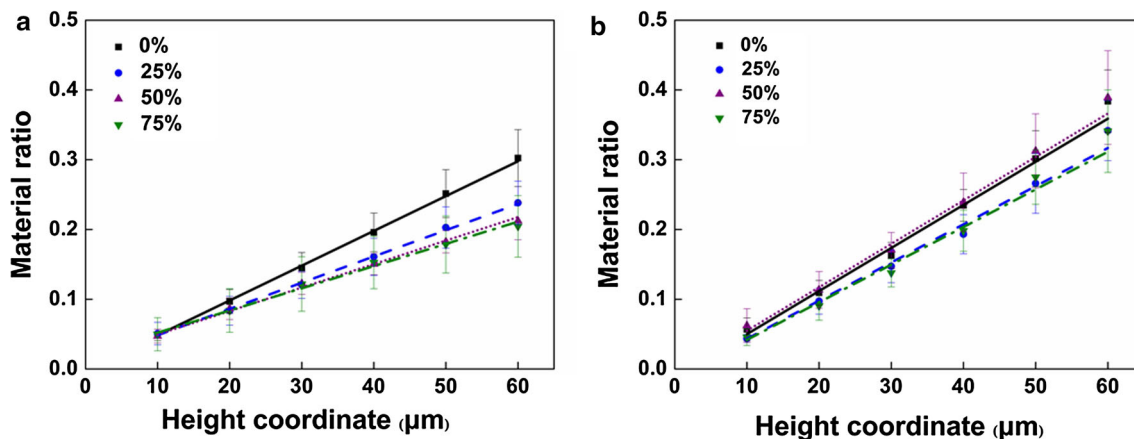


**Fig. 11** Material ratio of MCS surfaces as a function of height (measured from the top of the surface downwards) for samples stretched in **a** *p*-direction and **b** *i*-direction. Mean values and standard deviations of surface analyses with 10 images are shown together with linear fits

in the dry condition. This observation has been made by a number of studies [14].

The classical two-term friction model applied to polymers, textiles as well as human skin [23, 24] implies that the friction coefficient is the sum of two independent contributions due to adhesion and deformation, i.e.,  $\mu = \mu_{adh} + \mu_{def}$ . Although the deformation component

might be important for certain fibrous materials, the friction of textiles was found to be mainly determined by the adhesion friction component in recent studies [25, 26]. In the case of MCSs in contact with smooth PUR, the systematic decrease in friction coefficients as a function of normal force (Table 3; Fig. 12) also suggests the predominance of an adhesion friction mechanism, although

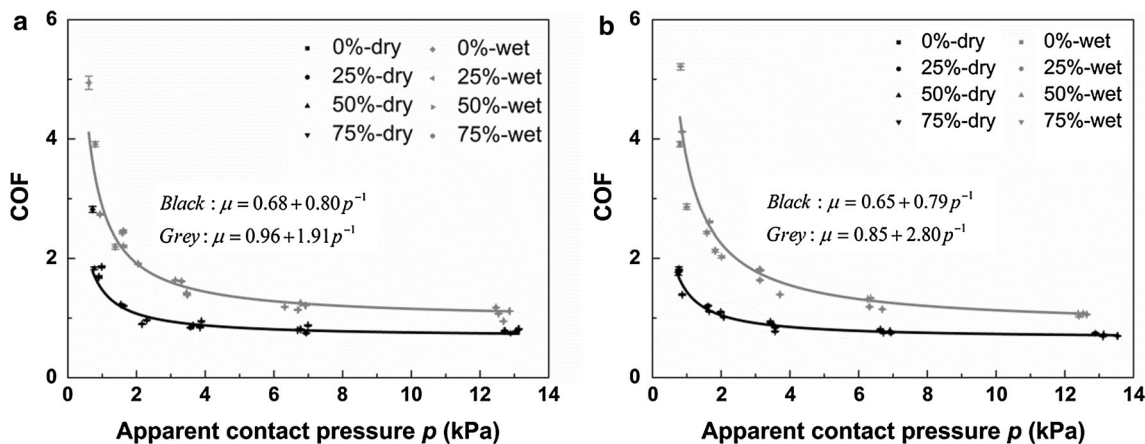


**Fig. 12** Friction coefficient of MCS samples sliding on smooth PUR as a function of the apparent contact pressure for strains in **a**  $p$ -direction and **b**  $i$ -direction together with fits according to Eq. (2)

superimposed small contributions due to deformation cannot be completely ruled out.

According to the adhesion friction model, the friction force can be expressed as  $F = \tau A_r$  where  $\tau$  denotes the interfacial shear strength and  $A_r$  the real contact area between two surfaces [27]. A common assumption for human skin is that the interfacial shear strength is a linear function of the form  $\tau = \tau_0 + \alpha p_r$  where  $\tau_0$  is the intrinsic shear strength,  $p_r$  the mean contact pressure and  $\alpha$  the pressure coefficient [23]. When writing  $p_r = N/A_r$  for the mean contact pressure, for the friction coefficient follows  $\mu = F/N = \alpha + \tau_0 p_r^{-1}$  [14]. While the apparent contact pressure  $p$  between MCS samples and the PUR surface in friction measurements is given by the applied normal load and the size of the textile samples, the mean contact pressure  $p_r$  resulting in the microscopic contact zones between MCS samples and skin model remains unknown. However, as the relationship between apparent and real contact pressure is  $p = (A_r/A) \cdot p_r$ , where  $A_r/A$  is the ratio between real and apparent contact area, the friction coefficient as a function of the apparent contact pressure can be expressed as

$$\mu(p) = \alpha + \tau_0 \frac{A_r}{A} p^{-1}. \tag{2}$$

Figure 12 shows measurement data for MCS samples together with data fits according to Eq. 2. The results for the unstretched MCS samples and stretched ones in  $p$ - and  $i$ -direction followed the same overall systematics. The fit parameters indicate that the pressure coefficient  $\alpha$  is a factor of about 1.4 higher under wet compared to dry conditions, whereas the product  $\tau_0(A_r/A)$  is increased by a factor of roughly 3 under wet conditions.

It is not possible to compare the values of the fit parameters shown in Fig. 12 with literature data, as no results are available for similar material combinations. The

observed pressure coefficients between 0.65 and 0.96, however, lie in the same order of magnitude as values found for the friction between human skin and other materials [15, 23]. A relatively low value of  $\alpha = 0.32$  was recently reported in a study on the friction between forearm skin and a bed sheet [28], and the product  $\tau_0(A_r/A)$  was found to be 1.1 which lies between the values for dry and wet conditions obtained in the present study as shown in Fig. 12.

#### 4.2 Compression and Contact Behavior of MCS Fabrics

The results on the macroscopic compression behavior of MCS fabric described in Sect. 3.2 indicated that for a normal force of 8 N, the compression of the MCS samples was between 131 and 154  $\mu\text{m}$  (Fig. 6), while the average penetration of the fabric surface asperities into the smooth PUR material is 12  $\mu\text{m}$  (Fig. 7). Qualitatively, it can be assumed that the textile structure is compressed as a whole and that during compression, the fabric surface is flattened to a certain degree while penetration into the PUR material at the same time occurs at high surface asperities. As there was no experimental technique available to observe the interface between the MCS fabrics and the PUR material during compression tests, it was neither possible to measure the deformation of the textile surface asperities nor to determine the microscopic contact area with the counter-surface.

In the following, two theoretical approaches based on the Hertz model are used to estimate and discuss the contact behavior between MCS fabrics and PUR on the microscopic level. While the first model considers the mechanical contact between a smooth surface and round asperities (surface peaks of the MCS fabrics), the second

model assumes contact between a smooth surface and cylindrical fibers (inlaid yarns of the MCS fabrics).

#### 4.2.1 Contact of Round Surface Asperities

It is interesting that the force deformation curves of compression tests shown in Figs. 4 and 6 could be fitted in good agreement with power functions with exponents of 3/2, because the same exponent would be expected within the framework of the Hertz contact model, which is widely used to study the elastic contact between a spherical body and a half-space and is also applicable to single asperities of a rough surface in contact with a smooth counter-surface [29].

The Hertz model for a sphere with radius  $R$  in contact with a half-space implies the following relationship between the deformation  $d$ , the radius  $a$  of the circular contact area, and the normal force  $N$ :  $d = \frac{a^2}{R} = \left(\frac{9}{16} \frac{N^2}{RE_c^2}\right)^{1/3}$ . The composite elastic modulus  $E_c$  is given by the elastic moduli  $E_{1,2}$  and Poisson's ratios  $\nu_{1,2}$  of the materials in contact. If one of the two materials is considerably softer than the other, the composite elastic modulus is mainly determined by the soft material and can be expressed as  $E_c \cong E_{\text{soft}} / (1 - \nu_{\text{soft}}^2)$ . Because the MCS fabrics appeared much softer than the PUR material in the compression tests, the composite elastic modulus is expected to be mainly determined by the properties of the textile.

Although a flat MCS sample in contact with a smooth PUR surface was investigated here, it can be assumed that the peaks of the fabric surface represent round asperities (due to the round yarn geometries) for which the Hertz contact model can be applied. Considering the textile surface as composed of  $n$  surface asperities characterized by the same average radius of curvature  $R_i$ , the deformation of

an individual asperity can be written as  $d_i = \left(\frac{9}{16} \frac{(N/n)^2}{R_i E_{ci}^2}\right)^{1/3}$ , where  $E_{ci}$  represents the composite elastic modulus of a single textile surface asperity in contact with PUR. Because the relationship between the local deformation behavior of surface asperities and the compression of the whole fabric is unknown, this parameter cannot be determined. However, due to the fact that the microscopic contact area between MCS fabrics and smooth PUR is much smaller than the apparent contact area, it is plausible to assume  $E_{ci} = f_E \cdot E_{\text{compr}}$  with  $f_E > 1$ .

The highest MCS surface asperities are located on top of the inlaid yarn and are probably formed by the thin filaments wrapped around the inlaid yarn (see Fig. 3). Thus, it can be assumed that the number of asperities  $n$  in contact with PUR is proportional to the density of inlaid yarns as well as to the inverse of the average distance  $\delta$  between thin filaments. If the length of inlaid yarns per unit area is denoted by  $l$ , the expressions above imply  $d_i \sim n^{-2/3} \sim (l/\delta)^{-2/3}$ . The effective radius of curvature  $R_i$  of MCS surface asperities can be estimated to be of the order of magnitude 80  $\mu\text{m}$  (square root of the product of the radii of the inlaid yarn and the filaments wrapped around it).

The length of inlaid yarns per unit area  $l$  and the average distance between surface asperities  $\delta$  vary due to the surface changes taking place when MCS fabrics are stretched in different directions (Sect. 3.3). Results of the analysis of microscopic images are given in Table 4. In addition, the table shows results for  $d_i$  and the ratio between real ( $A_r = nA_i$ ) and apparent contact area ( $A_{\text{app}} = 638 \text{ mm}^2$ ),

calculated on the basis of the expression  $d_i = \frac{a_i^2}{R_i} = \frac{A_i}{\pi R_i} = \left(\frac{9}{16} \frac{(N/n)^2}{R_i \cdot (f_E E_{\text{compr}})^2}\right)^{1/3}$  for a force of 8 N and using  $f_E = 34$ .

**Table 4** Geometrical parameters related to the surface asperities of MCS fabrics at various strains:  $l$  = length of inlaid yarns per unit area,  $\delta$  = average distance between thin filaments wrapped around the inlaid yarns,  $n$  = density of surface asperities associated with the tops of thin filaments

| MCS fabric             | $l$ (mm/mm <sup>2</sup> ) | $\delta$ (mm) | $n$ (mm <sup>-2</sup> ) | $E_{\text{compr}}$ (kPa) | $d_i$ ( $\mu\text{m}$ ) | $A_r/A_{\text{app}}$ (%) |
|------------------------|---------------------------|---------------|-------------------------|--------------------------|-------------------------|--------------------------|
| 0 % in $p$ -direction  | 1.897                     | 0.195         | 9.73                    | 114.2                    | 9.2                     | 2.2                      |
| 25 % in $p$ -direction | 1.494                     | 0.172         | 8.69                    | 103.0                    | 10.6                    | 2.3                      |
| 50 % in $p$ -direction | 1.234                     | 0.181         | 6.82                    | 91.8                     | 13.5                    | 2.3                      |
| 75 % in $p$ -direction | 1.093                     | 0.187         | 5.84                    | 80.6                     | 16.3                    | 2.4                      |
| 0 % in $i$ -direction  | 1.897                     | 0.195         | 9.73                    | 114.2                    | 9.2                     | 2.2                      |
| 25 % in $i$ -direction | 1.965                     | 0.217         | 9.06                    | 103.0                    | 10.3                    | 2.3                      |
| 50 % in $i$ -direction | 2.017                     | 0.249         | 8.10                    | 91.8                     | 12.0                    | 2.4                      |
| 75 % in $i$ -direction | 2.073                     | 0.307         | 6.75                    | 80.6                     | 14.8                    | 2.5                      |

When associating the contact of MCS surfaces with the contact of a large number of individual asperities and taking into account the elastic modulus of MCS samples determined in compression tests ( $E_{\text{compr}}$ ), the Hertz contact model provides estimates for the average vertical deformation of individual asperities  $d_i$  as well as the ratio between real and apparent contact area. In the last two columns, results are shown for a normal load of 8 N and  $E_{ci} = 34 \cdot E_{\text{compr}}$ . See text for details

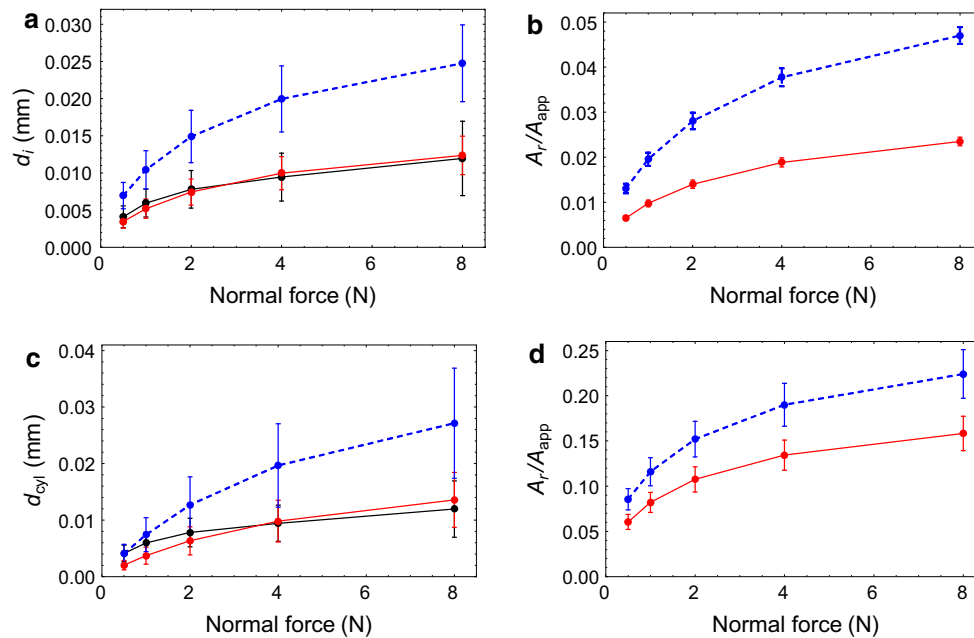


**Fig. 13** Comparison between the contact models for round surface asperities (*above*) and cylindrical fibers (*below*). **a** Average vertical deformation of MCS surface asperities  $d_i$  and **b** ratio between real and apparent contact area estimated on the basis of the Hertz contact model, thereby using the geometrical parameters summarized in Table 4 and  $R_i = 80 \mu\text{m}$  as effective radius of curvature of surface asperities. The *points and bars* indicate means and standard deviations for all investigated strain states, i.e., unstretched MCS samples and three different strains in both *p*- and *i*-direction. The *red curves* in **a** and **b** show results assuming  $E_{ci} = 34 \cdot E_{compr}$  for the elastic modulus at MCS surface asperities which are in good agreement with the data in Fig. 7 (*black curve*). The *blue curves* in **a** and **b** show results for

$E_{ci} = 12 \cdot E_{compr}$ , leading to a factor of 2 larger deformations and real contact areas. **c** Vertical deformation  $d_{cyl}$  of the inlaid yarns on MCS surfaces and **d** ratio between real and apparent contact area estimated on the basis of the cylindrical Hertz contact model, thereby using the data for  $l$  in Table 4 to calculate the length of the inlaid yarns with radius  $R = 180 \mu\text{m}$ . The *red curves* in **c** and **d** show results assuming  $E_{cyl} = 8 \cdot E_{compr}$  for the effective elastic modulus, being roughly comparable with the data in Fig. 7 (*black curve*). The *blue curves* in **c** and **d** show results for  $E_{cyl} = 4 \cdot E_{compr}$ , leading to a factor of 2 larger deformations and a factor of  $\sqrt{2}$  greater real contact areas (Color figure online)

For this specific value of  $f_E$ , the resulting average deformations  $d_i$  approximately correspond to the average differences seen in compression tests of MCS samples against PUR and steel, respectively (Fig. 7). The results for  $d_i$  and  $A_r/A_{app}$  shown in Table 4 scale with  $(N/f_E)^{-2/3}$  and can thus be used to determine values for other normal forces and factors  $f_E$ . Figure 13 shows a comparison between the data of Fig. 7 and Table 4 with results for  $f_E = 12$ , for which the average deformations  $d_i$  are a factor of 2 larger.

From the results in Table 4 and Fig. 13, it is evident that the parameters  $l$ ,  $\delta$ ,  $n$ ,  $E_{compr}$ ,  $d_i$  show significant systematic variations as a function of the strain state of the MCS fabrics. In contrast, the variations in the microscopic contact area at individual surface asperities  $A_i$  and the ratio  $A_r/A_{app}$  are small and depend only slightly on the strain state.

#### 4.2.2 Contact of Cylindrical Fibers

The inlaid yarns that represent an important feature of MCS surfaces (Fig. 3) can be considered as cylinders with

a radius of  $R = 180 \mu\text{m}$ . Therefore, a Hertz contact model based on cylindrical contact geometry is investigated here as an alternative to the model for round surface asperities described above. For a cylinder with radius  $R$  and length  $L$  in contact with a half-space, the vertical deformation as a function of the normal force  $N$  and the composite elastic modulus  $E_c$  is given by the equation  $d = \frac{4N}{\pi LE_c}$  and the contact area by the relationship  $A = 2L\sqrt{Rd}$  [29].

The total length of inlaid yarn within the fabric sample area can be calculated by  $L = l \cdot A_{app}$  using the data in Table 4. Writing  $E_c = f_E \cdot E_{compr}$  for the elastic modulus, it follows that the deformation scales with  $N/f_E$ , while the contact area scales with  $\sqrt{N/f_E}$ . It is found that for  $f_E = 8$ , the resulting average deformations  $d_{cyl}$  of the inlaid yarns lie in the range of the average differences seen in compression tests of MCS samples against PUR and steel, respectively (Fig. 13). For such deformations, the cylindrical Hertz model predicts 7–10 times larger real contact areas (Fig. 13d) than the model assuming round surface asperities (Fig. 13b).

### 4.3 Relationship Between Surface Topography and Friction Coefficients of MCS Fabrics

The analyses based on simple theoretical contact models in Sect. 4.2 showed that the microscopic contact areas between MCS fabrics and smooth PUR remain relatively constant for different strains even if considerable changes take place on the MCS surfaces. This finding is consistent with the observation of friction coefficients that are practically independent of the strain state of the fabrics and strongly supports the applicability of the adhesion friction model, according to which the friction force is proportional to the real contact area.

The red curves shown in Fig. 13 can be interpreted as lower limits for the deformations and real contact areas of the MCS surfaces during mechanical contact against smooth PUR. For deformations of 10  $\mu\text{m}$ , the Hertz model for round asperities (corresponding to the peaks of the filaments wrapped around the inlaid yarn) indicates a real contact area of the order of magnitude of 2 % of the apparent contact area, while the Hertz model for cylindrical contact geometry (corresponding to the inlaid yarns) predicts a value around 13 %. In reality, the deformations of the investigated fabrics were probably larger and could have been closer to the blue curves in Fig. 13, representing an increase in deformation by a factor of 2 compared to the red curves. For deformations between 20 and 25  $\mu\text{m}$ , the model for round asperities indicates a real contact area of 4–5 % and the cylindrical model values between 18 and 21 %.

The fact that the asperity contact model is in good qualitative agreement with the differences observed in the deformation of MCS samples when compressed against PUR and steel (Figs. 7, 13) is a strong argument that this model offers an appropriate description of the contact behavior of MCS surfaces. Independently, the analysis of the microscopic surface topography of MCS fabrics provides additional information on the relationship between vertical deformation (penetration or compression) and real contact area, associated with the material ratio shown in Fig. 11. While deformations of 10  $\mu\text{m}$  indicate real contact areas around 5 %, deformations from 20 to 25  $\mu\text{m}$  suggest real contact areas in the range of 8–15 %. These values lie between those predicted by the two investigated contact models and thus confirm the realistic order of magnitude of the obtained results.

### 4.4 Limitations and Outlook

The experimental techniques applied for friction and compression measurements are well established and characterized by measurement uncertainties of a few percent. The vertical resolution of the digital microscope was high enough to measure surface profiles showing the

characteristic features governed by the fabric structure and constituent fibers, while in the analysis of the textile surface topographies, the height data were averaged over the whole microscopic images to determine material ratios. An uncertainty in the experimental methods was related to the preparation of MCS samples with defined strains in *p*- and *i*-direction. We estimated that the manual procedure allows an accuracy of about 5 %.

The analysis of the contact and friction behavior following Hertz theory involves the translation of macroscopic compression properties of MCS samples into micro-elastic properties associated with individual surface asperities of the fabrics. While compressive elastic moduli could be derived from compression tests with fabric samples, there was neither a method available to measure force–deformation curves for single fabric surface asperities nor a microscopic method to observe indentation and possible geometrical changes of surface asperities or the porous textile structure during mechanical contact with the skin model. Therefore, scaling factors were used here to estimate the micro-elastic properties of textile surface asperities from fabric compression measurements. The application or development of appropriate microscopic techniques would be interesting for future work in order to confirm or to improve the models used in the present study and to refine the approach for determining crucial contact mechanical parameters such as the real or microscopic contact area between two surfaces.

## 5 Conclusions

The relationship between microscopic surface properties and macroscopic contact and friction behavior of a MCS was investigated. The application of different strains to fabric samples significantly changed the surface topography and slightly influenced the compression properties, while not affecting the friction behavior against a smooth skin model. The strain-independent friction behavior can be explained by the fact that the strain-induced changes in surface topography and compression properties have a balancing effect and lead to a relatively constant real contact area on the microscopic level. It was found that the friction behavior of the MCS is in accordance with the adhesion friction model and that the contact behavior on the microscopic level can be theoretically described by assuming the fabric surface to be composed of numerous round asperities obeying the Hertz contact model. The new insights might be useful to improve medical textiles by optimizing their design on the microscopic level.

**Acknowledgments** We thank Emilie Bertaux Hegemann for valuable discussions and background information on medical compression

stockings and Sigvaris AG, St. Gallen, for kindly providing samples of medical compression stockings. The first author acknowledges the support of the CSC Scholarship from the Ministry of Education of P. R. China. Part of work was funded by the National Natural Science Foundation through project (No. 51175076).

## References

- O'Meara, S., Cullum, N., Nelson, E.A., Dumville, J.C.: Compression for venous leg ulcers. *Cochrane Database Syst. Rev.* **11**, CD000265 (2012). doi:[10.1002/14651858.CD000265.pub3](https://doi.org/10.1002/14651858.CD000265.pub3)
- Partsch, B., Partsch, H.: Compression stockings for treating venous leg ulcers: measurement of interface pressure under a new ulcer kit. *Phlebology* **23**(1), 40–46 (2008)
- Wienert, V., Gerlach, H., Gallenkemper, G., Kahle, B., Marshall, M., Rabe, E., Stenger, D., Stücker, M., Waldermann, F., Zabel, M.: Medical compression stocking (MCS). *Journal der Deutschen Dermatologischen Gesellschaft* **6**(5), 410–415 (2008)
- Ali, A., Creasy, R.H., Edge, J.A.: Physiological effects of wearing graduated compression stockings during running. *Eur. J. Appl. Physiol.* **109**(6), 1017–1025 (2010)
- Cullum, N., Fletcher, A., Semlyen, A., Sheldon, T.A.: Compression therapy for venous leg ulcers. *Qual. Health Care* **6**(4), 226–231 (1997)
- Hsieh, H.F., Lee, F.P.: Graduated compression stockings as prophylaxis for flight-related venous thrombosis: systematic literature review. *J. Adv. Nurs.* **51**(1), 83–98 (2005)
- Morris, R.J., Woodcock, J.P.: Evidence-based compression: prevention of stasis and deep vein thrombosis. *Ann. Surg.* **239**(2), 162–171 (2004)
- Van Geest, A.J., Franken, C.P.M., Neumann, H.A.M.: Medical elastic compression stockings in the treatment of venous insufficiency. In: Elsner, P., Hatch, K., Wigger-Alberti, W. (eds.) *Textile and the Skin. Current Problems in Dermatology*, pp. 98–107. Karger, Basel (2003)
- Partsch, H.: Venous thromboembolic diseases. *Phlebolympnologie* **18**(2), 53–120 (2011)
- Hafner, J., Lüthi, W., Hänsle, H., Kammerlander, G., Burg, G.: Instruction of compression therapy by means of interface pressure measurement. *Dermatol. Surg.* **26**(5), 481–487 (2000)
- Liu, R., Kwok, Y.L., Li, Y., Lao, T.T., Zhang, X.: Skin pressure profiles and variations with body postural changes beneath medical elastic compression stockings. *Int. J. Dermatol.* **46**(5), 514–523 (2007)
- Wang, Y., Zhang, P., Feng, X., Yao, Y.: New method for investigating the dynamic pressure behavior of compression garment. *Int. J. Cloth. Sci. Technol.* **22**(5), 374–383 (2010)
- Zhang, X., Yeung, K.W., Li, Y.: Numerical simulation of 3D dynamic garment pressure. *Text. Res. J.* **72**(3), 245–252 (2002)
- Derler, S., Gerhardt, L.-C.: Tribology of skin: review and analysis of experimental results for the friction coefficient of human skin. *Tribol. Lett.* **45**(1), 1–27 (2012)
- Hendriks, C.P., Franklin, S.E.: Influence of surface roughness, material and climate conditions on the friction of human skin. *Tribol. Lett.* **37**(2), 361–373 (2010)
- Skedung, L., Danerlöv, K., Olofsson, U., Aikala, M., Niemi, K., Kettle, J., Rutland, M.W.: Finger friction measurements on coated and uncoated printing papers. *Tribol. Lett.* **37**(2), 389–399 (2010)
- Tomlinson, S.E., Lewis, R., Carré, M.J.: The effect of normal force and roughness on friction in human finger contact. *Wear* **267**(5–8), 1311–1318 (2009)
- Masen, M.A.: A systems based experimental approach to tactile friction. *J. Mech. Behav. Biomed. Mater.* **4**(8), 1620–1626 (2011)
- RAL Deutsches Institut für Gütesicherung und Kennzeichnung e. V.: *Medical compression hosiery—Quality assurance RAL-GZ 387/1* (2008)
- Gerhardt, L.-C., Mattle, N., Schrade, G.U., Spencer, N.D., Derler, S.: Study of skin-fabric interactions of relevance to decubitus: friction and contact-pressure measurements. *Skin Res. Technol.* **14**(1), 77–88 (2008)
- Derler, S., Schrade, U., Gerhardt, L.-C.: Tribology of human skin and mechanical skin equivalents in contact with textiles. *Wear* **263**(7–12), 1112–1116 (2007)
- Derler, S., Rotaru, G.-M., Ke, W., El Issawi-Frischknecht, L., Kellenberger, P., Scheel-Sailer, A., Rossi, R.M.: Microscopic contact area and friction between medical textiles and skin. *J. Mech. Behav. Biomed. Mater.* **38**, 114–125 (2014)
- Adams, M.J., Briscoe, B.J., Johnson, S.A.: Friction and lubrication of human skin. *Tribol. Lett.* **26**(3), 239–253 (2007)
- Gupta, B.S.: *Friction in Textile Materials*. CRC Press, Boca Raton, FL (2008)
- Bueno, M.A., Bocquet, R., Turlonias, M., Rossi, R.M., Derler, S.: Study of friction mechanisms of hairy textile fabrics. *Wear* **303**(1–2), 343–353 (2013)
- Rotaru, G.-M., Pille, D., Lehmeier, F.K., Stämpfli, R., Scheel-Sailer, A., Rossi, R.M., Derler, S.: Friction between human skin and medical textiles for decubitus prevention. *Tribol. Int.* **65**, 91–96 (2013)
- Bowden, F.P., Tabor, D.: *The Friction and Lubrication of Solids*. Clarendon Press, Oxford (1986)
- Derler, S., Rossi, R.M., Rotaru, G.-M.: Understanding the variation of friction coefficients of human skin as a function of skin hydration and interfacial water films. *Proc. Inst. Mech. Eng. Part J: J. Eng. Tribol.* (2014). doi:[10.1177/1350650114527922](https://doi.org/10.1177/1350650114527922)
- Popov, V.L.: *Contact Mechanics and Friction: Physical Principles and Applications*. Springer, Berlin (2010)